# Scattering Analysis of Flat Electric Dipoles on Multilayer Chiral Structures

N. R. Rabelo[*], S. J. S. Sant'Anna[*+], J. C. da S. Lacava[*], D. Fernandes[*]

*Laboratório de Antenas e Propagação, Instituto Tecnológico de Aeronáutica
Praça Mal. Eduardo Gomes, 50, CEP 12228-900, São José dos Campos-SP, Brazil
{lacava, david}@ita.br; nrrabelo@yahoo.com

+Divisão de Processamento de Imagem, Instituto Nacional de Pesquisas Espaciais
Av. dos Astronautas, 1758, CEP 12227-010, São José dos Campos-SP, Brazil
sidnei@dpi.inpe.br

***Abstract*— Identification of natural targets out of polarimetric SAR data can be made from their scattering matrices, once they are determined. The methodology outlined here permits the spectral domain analysis of a confined chiral layer stacked up between free space and ground, containing flat electric and magnetic elements at any layer interface, and illuminated by an elliptically polarized plane wave at oblique incidence. From the closed-form field expressions so obtained, scattering parameters, including the scattering matrix, of an electric dipole atop the chiral layer are readily determined and analyzed.**

## I. Introduction

There has been a growing interest in retrieving and identifying the characteristic parameters from natural targets out of full polarimetric SAR data resulting from microwave remote sensing. Data analysis can be performed using polarimetric decomposition techniques, which are based on the characterization of radar scattering from complex targets in terms of a linear combination of scattering from simpler ones [1].

In this context, the scattering matrix computation plays a central role in extracting information from polarimetric SAR data. From the knowledge of the scattering matrix, mathematical models for natural targets and other polarimetric target descriptors can be obtained [2].

Natural targets can exhibit anisotropic or chiral characteristics. Scattering from some anisotropic natural targets has been discussed in [3] and chirality effects in radar remote sensing data from certain types of vegetation have been considered in [4].

The electromagnetic mathematical model developed in [5]-[7] for the study of scattering from multiple isotropic planar layers containing flat electrical and magnetic elements at the layer interfaces can be extended to anisotropic and chiral media, though at the cost of added complexity. Using this methodology, an analytical closed-form expression is derived for the scattering matrix of electric dipoles embedded in a three-layer planar structure, with a chiral layer in between, illuminated by an elliptically polarized plane wave at oblique incidence. As an application of these results, the structure's directivity function and polarimetric response are also analyzed.

## II. Theory

The structure under investigation, as depicted in Fig. 1, consists of a confined chiral layer stacked up in the $z$ direction between free space (the upper layer) and ground (the lower layer), both linear, isotropic and homogenous. All three layers are assumed to be planar and unbounded along the transversal $x$ and $y$ directions. The ground layer, occupying the negative-$z$ region, has complex permittivity $\varepsilon_g$ and complex permeability $\mu_g$. The chiral layer of thickness $d$ is characterized by complex permittivity $\varepsilon$, complex permeability $\mu$, and chiral admittance $\zeta$. Perfect electric conductors of infinitesimal thickness, acting as the virtual sources of the scattered fields, are supposed to exist on each layer interface, at $z = 0$ and $z = d$.

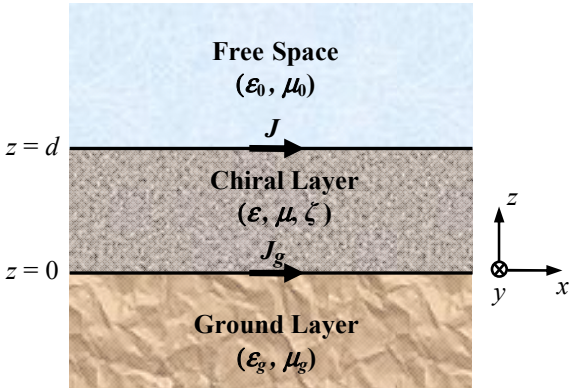


Fig. 1 Chiral layer between free space and ground.

The analytical development is based on a global rectangular coordinate system located atop the ground layer ($z = 0$). The electromagnetic fields in each of the three layers can be determined following the methodology described in [7], whereby the structure is treated as a boundary value problem, and the analysis is carried out using the spectral domain full-wave technique. The surface electric current densities on the conductors located at the interfaces are induced by an illuminating elliptically polarized plane wave at oblique incidence. The solution for the electromagnetic fields in any of the three layers takes the following steps:

- The wave equations for each layer are solved in the Fourier domain, resulting in a system of differential equations;
- Application of the proper electromagnetic boundary conditions at each interface yields a set of eight linear equations in terms of the longitudinal ($z$) components of the spectral fields;
- Analytical solution of the system of linear equations leads to the spectral Green's functions in closed form;
- From the Green's functions and the transformed surface current densities on the conductors, the spectral fields at any point of the multilayer structure can be determined.
- Finally, the electromagnetic fields in the space domain are obtained from the inverse double Fourier transform.

Note the approach described above is general and can be directly extended to any number of chiral layers.

For the purpose of scattering analysis, interest is on the far electromagnetic fields scattered into free space by the multilayer structure. In this particular case, the scattered wave can be approximated [1] by a plane wave at the receiving antenna, considered sufficiently small, so the Stationary Phase Method [8] can be used to obtain their asymptotic expressions, resulting in:

$$\boldsymbol{E}_0(r,\theta,\phi) \cong -\frac{ik_0}{2\pi}\frac{e^{-ik_0 r}}{r}\cot\theta\{e_{0z}(k_{xe},k_{ye})\boldsymbol{\theta} - \eta_0 h_{0z}(k_{xe},k_{ye})\boldsymbol{\phi}\} \quad (1)$$

in the spherical coordinate system, where boldface letters represent vectors, $\eta_0$ is the intrinsic impedance of free space, $k_0$ is the wave number in vacuum of the excitation wave, $k_{xe} = k_0 \sin\theta\cos\phi$ and $k_{ye} = k_0 \sin\theta\sin\phi$ define the stationary phase point, $r$ is the distance between the receiving antenna and the target, and $e_{0z}$ and $h_{0z}$ are the longitudinal components of the spectral electromagnetic fields in free space, as determined by the method previously outlined.

From this result and the knowledge of the electric current densities on the interfaces, the scattering matrix elements can then be completely determined for any incidence and scattering direction.

Considering an electric conductor located at the interface between the chiral layer and free space (i.e. at $z = d$), the amplitudes of the far spectral electromagnetic fields scattered into free space are given by:

$$e_{0z}(k_x,k_y) = \frac{e^{i\Psi_0(k_x,k_y)}}{4\Delta(k_x,k_y)}\left[\Theta(k_x,k_y)j_x(k_x,k_y) + \Theta(k_y,-k_x)j_y(k_x,k_y)\right], \quad (2)$$

$$h_{0z}(k_x,k_y) = \frac{e^{i\Psi_0(k_x,k_y)}}{4\omega\Delta(k_x,k_y)}\left[\Phi(k_x,k_y)j_x(k_x,k_y) + \Phi(k_y,-k_x)j_y(k_x,k_y)\right], \quad (3)$$

where $j_x$ and $j_y$, the Fourier transforms of the surface electric current density on the conductor, can be numerically computed from a system of integral equations via the Method of Moments, using subdomain base functions and identical test functions (Galerkin Method), or via other equivalent techniques. The closed-form functions $\Theta$, $\Phi$, $\Delta$, and $\psi_0$, are defined by:

$$\begin{aligned}\Theta(k_x,k_y) = 8\omega\mu\{&\beta_5\gamma_1\gamma_2 k_x[\gamma_0(\alpha_2 + \alpha_1\cos\psi_1\cos\psi_2) \\ &+ 2q^2\mu_0\gamma_g\cos\psi_1\cos\psi_2] + \sin\psi_1\cos\psi_2[\beta_2\beta_4\beta_5 \\ &+ i\gamma_1\gamma_2(\beta_1\beta_6 q + \alpha_1\beta_3\mu_0 k_x)] + \cos\psi_1\sin\psi_2[i\beta_1\beta_3\beta_5 \\ &+ \gamma_1\gamma_2(\beta_2\beta_7 q + i\alpha_1\beta_4\mu_0 k_x)] - \tfrac{1}{2}\sin\psi_1\sin\psi_2 \\ &\times[\alpha_1\gamma_g(\beta_1 k_e^2\gamma_1^2 - i\beta_2 k_d^2\gamma_2^2) + 4k_g^2 q^2\gamma_1^2\gamma_2^2\mu_0\mu k_x]\}\end{aligned} \quad (4)$$

$$\begin{aligned}\Phi(k_x,k_y) = 8\omega\mu\{&k^2\gamma_1\gamma_2\mu k_y[\omega^2\varepsilon_0\gamma_g(\alpha_2 + \alpha_1\cos\psi_1\cos\psi_2) \\ &+ 2k_g^2 q^2\gamma_0\cos\psi_1\cos\psi_2] + \sin\psi_1\cos\psi_2[i\beta_6\beta_9 q\gamma_1\gamma_2 \\ &+ \beta_4(\beta_5\beta_8 + i\alpha_1 k^2\gamma_0 k_y)] + \cos\psi_1\sin\psi_2[\beta_7\beta_8 q\gamma_1\gamma_2 \\ &+ i\beta_3(\beta_5\beta_9 + \alpha_1 k^2\gamma_0 k_y)] - 0.5\sin\psi_1\sin\psi_2[\alpha_1\gamma_g \\ &\times(\beta_9 k_e^2\gamma_1^2 - i\beta_8 k_d^2\gamma_2^2) + 4\beta_5^2 q^2\gamma_0 k_y/\mu]\}\end{aligned} \quad (5)$$

$$\begin{aligned}\Delta(k_x,k_y) = i2\{&ik^2\gamma_1\gamma_2[\alpha_2\alpha_4\gamma_0\gamma_g - \cos\psi_1\cos\psi_2(\alpha_1\alpha_3\gamma_0\gamma_g \\ &+ 2q^2\mu^2(k_g^2\gamma_0^2 + k_0^2\gamma_g^2))] + \gamma_2 q\mu\sin\psi_1\cos\psi_2[\alpha_1\gamma_g \\ &\times(k_e k_0^2\gamma_1^2 + k_d k^2\gamma_0^2) + \alpha_3\gamma_0(k_e k_g^2\gamma_1^2 + k_d k^2\gamma_g^2)] \\ &+ \gamma_1 q\mu\cos\psi_1\sin\psi_2[\alpha_1\gamma_g(k_e k^2\gamma_0^2 + k_d k_0^2\gamma_2^2) \\ &+ \alpha_3\gamma_0(k_e k^2\gamma_g^2 + k_d k_g^2\gamma_2^2)] + i\,0.5\sin\psi_1\sin\psi_2 \\ &\times[\alpha_1\alpha_3\gamma_0\gamma_g(k_e^2\gamma_1^2 + k_d^2\gamma_2^2) + (2q\mu)^2((k_0 k_g\gamma_1\gamma_2)^2 \\ &+ (k^2\gamma_0\gamma_g)^2)]\}\end{aligned} \quad (6)$$

where:

$k_0 = \omega\sqrt{\mu_0\varepsilon_0}$ , $k = \omega\sqrt{\mu\varepsilon}$ , $k_g = \omega\sqrt{\mu_g\varepsilon_g}$ , $p = \omega\mu\zeta$ ,

$q = \sqrt{k^2 + p^2}$ , $k_d = p + q$ , $k_e = q - p$ , $u^2 = k_x^2 + k_y^2$ ,

$\gamma_0 = \sqrt{k_0^2 - u^2}$ , $\gamma_1 = \sqrt{k_d^2 - u^2}$ , $\gamma_2 = \sqrt{k_e^2 - u^2}$ , $\gamma_g = \sqrt{k_g^2 - u^2}$ ,

$\psi_0 = \gamma_0 d$ , $\psi_1 = \gamma_1 d$ , $\psi_2 = \gamma_2 d$ , $\alpha_1 = q^2\mu_g + \omega^2\varepsilon_g\mu^2$ ,

$\alpha_2 = q^2\mu_g - \omega^2\varepsilon_g\mu^2$ , $\alpha_3 = q^2\mu_0 + \omega^2\varepsilon_0\mu^2$ ,

$\alpha_4 = q^2\mu_0 - \omega^2\varepsilon_0\mu^2$ , $\beta_1 = \mu\gamma_0 k_x + iq\mu_0 k_y$ ,

$\beta_2 = i\mu\gamma_0 k_x + q\mu_0 k_y$ , $\beta_3 = k_e q\gamma_1\gamma_g$ , $\beta_4 = k_d q\gamma_2\gamma_g$ ,

$\beta_5 = k^2\mu\gamma_g$ , $\beta_6 = k_e k_g^2\mu\gamma_1$ , $\beta_7 = k_d k_g^2\mu\gamma_2$ ,

$\beta_8 = q\gamma_0 k_x + i\omega^2\varepsilon_0\mu k_y$ , $\beta_9 = iq\gamma_0 k_x + \omega^2\varepsilon_0\mu k_y$ .

Note that the spectral surface electric current densities $j_x$ and $j_y$, and functions $\Delta$, $\psi_0$, $\Theta$ and $\Phi$ are evaluated at the stationary phase point when used in eq. (1).

## III. Scattering Analysis

From the far electric field expression, eq. (1), it is possible to derive scattering attributes, such as the directivity function, the scattering matrix, and the polarimetric response, among others. The following analysis applies to the structure depicted in Fig. 1.

### *A. Directivity Function*

From antenna theory, the directivity function $D(\theta,\phi)$ is defined as the ratio of the radiation intensity $U(\theta,\phi)$ in a given direction to the average intensity radiated over all directions (i.e., an equivalent isotropic antenna), namely:

$$D(\theta,\phi)=\frac{4\pi\,U(\theta,\phi)}{P_i}\,, \tag{7}$$

where $P_i$ represents the average radiated power, and $U(\theta,\phi)$ for the three-layer structure of Fig. 1 is derived from eq. (1) as

$$U(\theta,\phi)=\frac{1}{2\eta_0}\left(\frac{k_0\cot\theta}{2\pi}\right)^2\left\{\left|e_{0z}(k_{xe},k_{ye})\right|^2+\eta_0^2\left|h_{0z}(k_{xe},k_{ye})\right|^2\right\}. \tag{8}$$

The directivity function for the structure of Fig. 1, with a short electric dipole located atop the chiral layer and characterized by $d=32$ mm, $\varepsilon=2\varepsilon_0$, $\varepsilon_g=\varepsilon_0$, $\mu=\mu_g=\mu_0$, loss tangents $\tan\delta=3.0\times10^{-4}$ (chiral layer) and $\tan\delta_g=1.0\times10^{-2}$ (ground layer), was evaluated at 1.25 GHz. The resulting three-dimensional graphics of $D(\theta,\phi)$ are illustrated in Fig. 2 for four values of the chiral admittance ($\zeta=0.0$, 3.0, 6.0, and 9.0 mS), the particular case of $\zeta=0.0$ mS corresponding to an achiral medium.

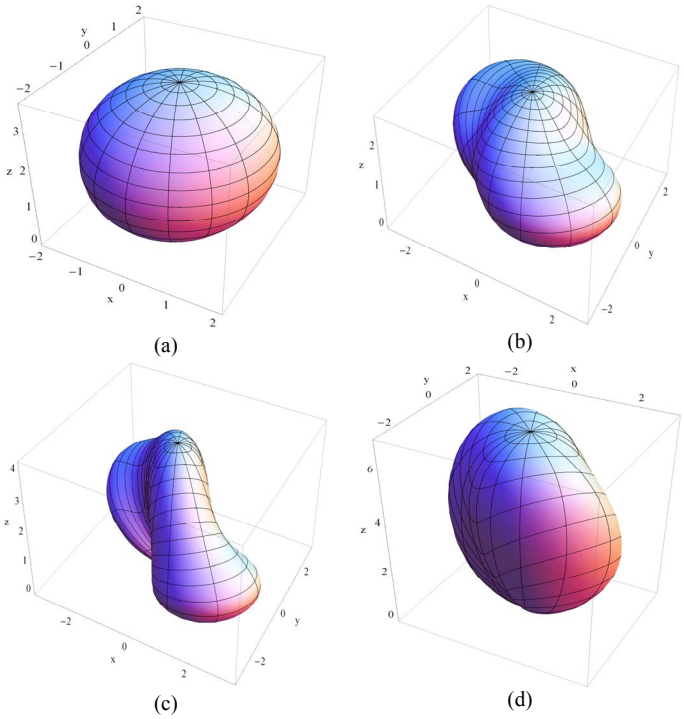


Fig. 2 Directivity function $D(\theta,\phi)$ 3-D patterns for a short electric dipole atop the chiral layer: (a) $\zeta=0.0$ mS, (b) $\zeta=3.0$ mS, (c) $\zeta=6.0$ mS, (d) $\zeta=9.0$ mS.

It is noticed from Fig. 2 that the shape and the values of the radiation peaks of the directivity patterns (idem the scattering radiation patterns) vary significantly according to the chirality (represented by the chiral admittance) of the confined layer. This is further evidenced by the directivity function cuts at the plane $\theta=45°$ shown in Fig. 3. Thus the directivity pattern can in principle be utilized as an indicator of the degree of chirality of the confined layer. Furthermore, one also notes that chirality impinges a rotation of the directivity (or radiation) pattern axis of maximum radiation value. Taking the achiral case as a reference, the axis rotation angles for chiral admittances of 3.0, 6.0 and 9.0 mS are respectively –35º, –43º and –67º.

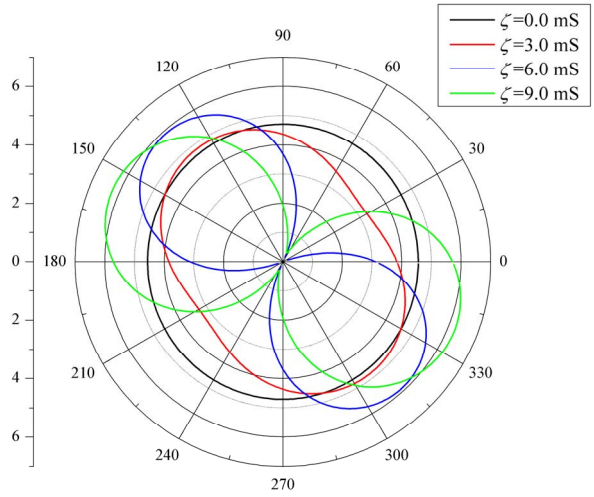


Fig. 3 Directivity function $D(\theta,\phi)$ cuts at the plane $\theta=45°$ for a short electric dipole atop the chiral layer.

To further evaluate the chirality effect, the directivity of a short electric dipole was computed for three different values of the chiral layer thickness ($d=16$, 24 and 32 mm). The influence of the thickness $d$ over the directivity is depicted in Fig. 4, which indicates that the structure's radiation pattern tends to be more directive as $d$ increases.

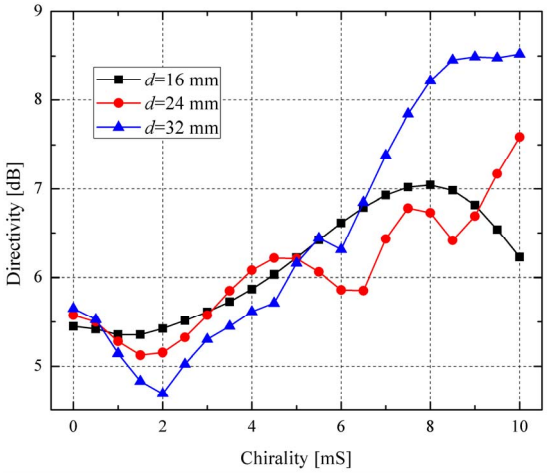


Fig. 4 Directivity of a short electric dipole atop the chiral layer for three values of the layer thickness.

*B. Scattering Matrix*

The scattering matrix can be regarded as the mathematical signature of a scattering target, as it relates the scattered wave's electric field to that of the incident wave. It is a comprehensive parameter in polarimetric SAR analysis, providing complete information about the scattering mechanism and from which other polarimetric features used to describe the scattering target can be derived.

The scattering matrix can be calculated following the procedure utilized in [5]. It is worth mentioning that the standard spherical coordinate system $(r, \theta, \phi)$ is directly related to the vertical and horizontal polarization system $(k, v, h)$, as described in [1].

The currents induced on the scattering elements depend on the incident wave polarization being horizontal or vertical. The following relation between the amplitudes of the far spectral electromagnetic fields scattered into free space, due to each linear polarization, can be obtained based on reciprocity:

$$e_{0z}^{(h)}(k_{xe}, k_{ye}) = -\eta_0 h_{0z}^{(v)}(k_{xe}, k_{ye}) \,, \tag{9}$$

where the superscripts ($v$, $h$) are associated with the vertical and horizontal polarization of the incident wave.

With that, the scattering matrix in the case of an electric dipole located at the interface between the chiral layer and free space can be calculated as

$$[S_{ed}] = Q_2 \begin{bmatrix} 1/Q_1 & -1 \\ -1 & Q_1 \end{bmatrix}, \tag{10}$$

where

$$Q_1 = [\eta_0 \Phi(k_{xe}, k_{ye})]/[\omega \Theta(k_{xe}, k_{ye})] \,, \tag{11}$$

$$Q_2 = -ie^{i\psi_0} \frac{\mu_0}{8\pi} \frac{\Phi(k_{xe}, k_{ye})}{\Delta(k_{xe}, k_{ye})} j_x^{(v)}(k_{xe}, k_{ye}) \cot\theta \,. \tag{12}$$

For validation purposes, the scattering matrix so obtained has been shown to reduce to the one described in [5]-[6] for the particular case of a three-layer achiral structure.

*C. Polarimetric Response*

Another way to characterize the scattering properties of a target is through its polarimetric response. This is a graphical representation of the target scattering cross section as a function of the ellipticity and the orientation angles of the transmitted electromagnetic wave [9]. The polarimetric response can be directly computed from the target's scattering matrix, once it is determined.

Therefore, from the scattering matrix derived above, eqs. (10) - (12), the polarimetric response of the three-layer structure shown in Fig.1 can be computed and analyzed. As an illustration, Figs. 5 and 6 show respectively the co-polarized and the cross-polarized cases of the polarimetric response of the structure whose characteristic parameters are as defined in Section III.A. Shown in these figures are the surface of the polarimetric response as well as its respective contour graphic for four values of the chiral admittance, the same used in Fig. 2 (i.e. $\zeta = 0.0$, 3.0, 6.0, and 9.0 mS). The maximum value of the co-polarized response is indicated on the contour graphic by the intersection of the two dashed lines.

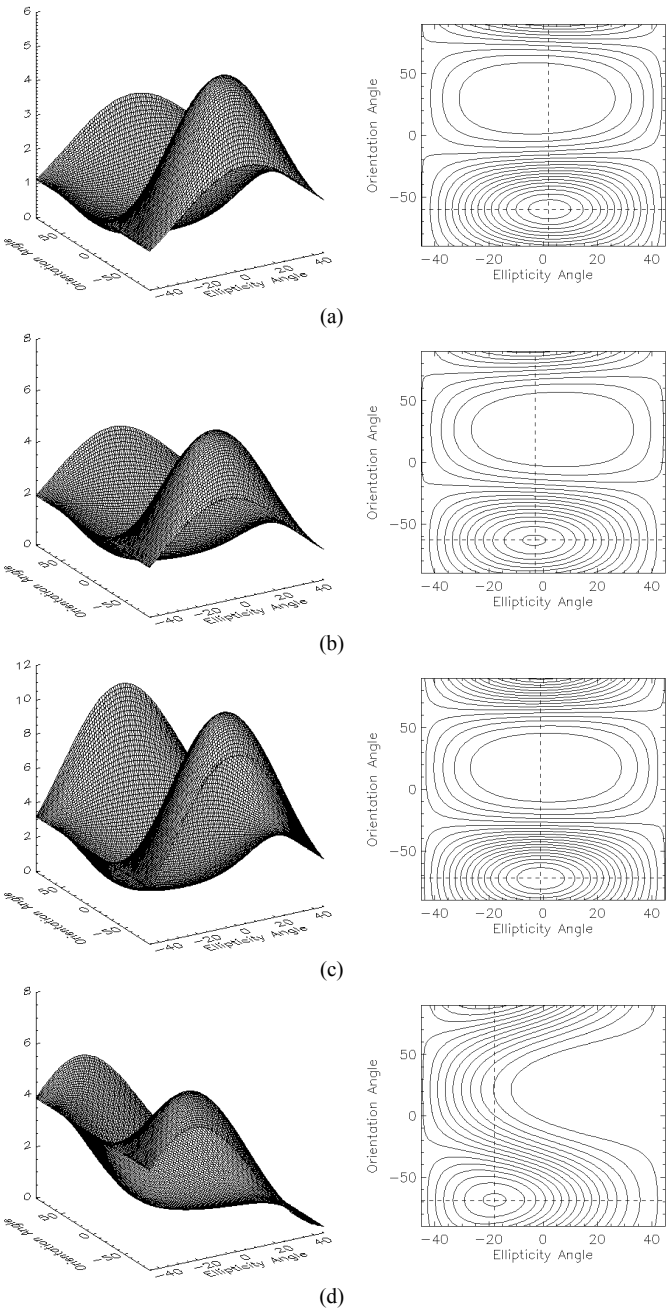


Fig. 5 Co-polarized case of the polarimetric response of a short electric dipole atop the chiral layer: (a) $\zeta = 0.0$ mS, (b) $\zeta = 3.0$ mS, (c) $\zeta = 6.0$ mS, (d) $\zeta = 9.0$ mS.

As in the case of the directivity function previously considered, it is evident from Figs. 5 and 6 that the chirality (represented by the chiral admittance) of the confined layer affects the characteristics of the co-polarized and the cross-polarized polarimetric responses of the structure. The analysis of the co-polarized polarimetric response shows that its point of

maximum as a function of the chiral admittance generates the blue line (triangular marker) locus drawn in Fig. 7.

Varying the chiral layer thickness ($d$ = 16, 24 and 32 mm), the shapes of the polarimetric response (co- and cross-polarized) remained similar, but the loci of the points of maximum changed considerably, as illustrated in Fig. 7

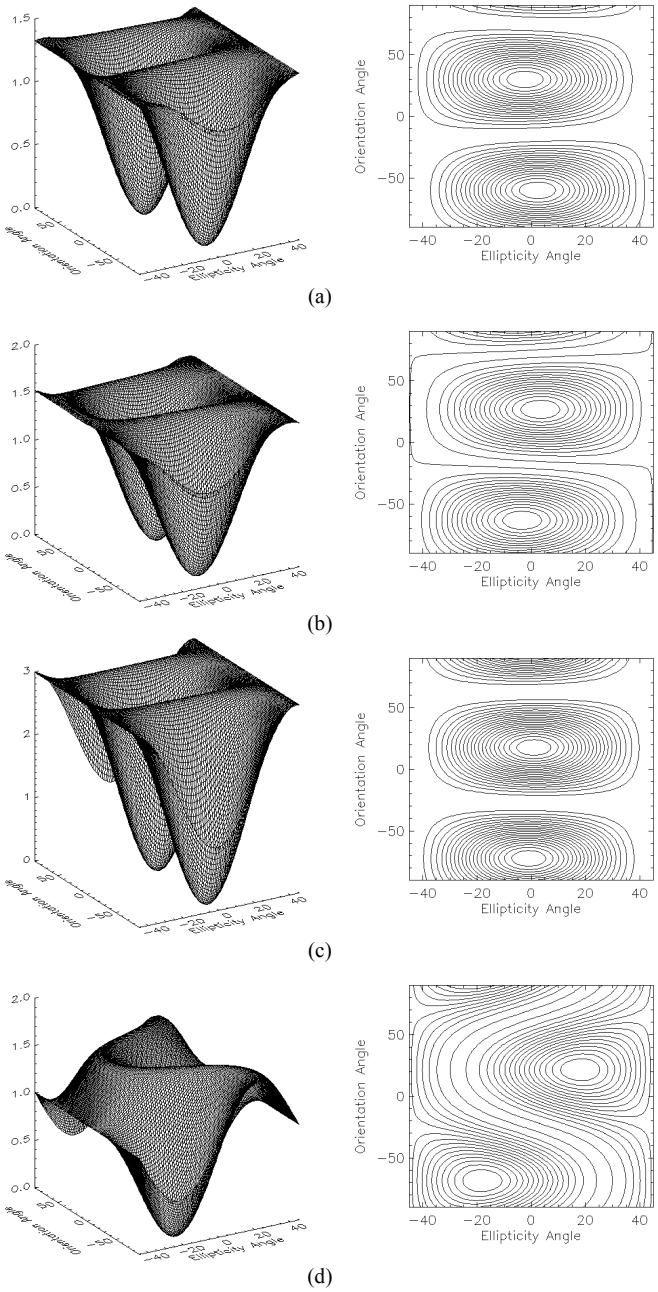


Fig. 6 Cross-polarized case of the polarimetric response of a short electric dipole atop the chiral layer: (a) $\zeta$ = 0.0 mS, (b) $\zeta$ = 3.0 mS, (c) $\zeta$ = 6.0 mS, (d) $\zeta$ = 9.0 mS.

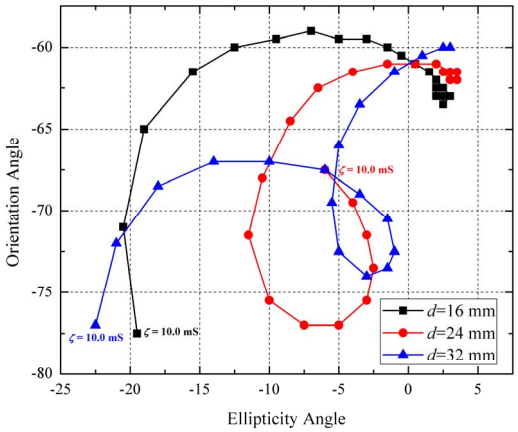


Fig. 7 Loci of the points of maximum of the co-polarized response of a short electric dipole atop the chiral layer for three values of the layer thickness.

## IV. Conclusion

The methodology previously developed for the computation of the electromagnetic fields in multilayer achiral structures can be extended to chiral media. Either type of scattering elements, electric and/or magnetic, can be present at any layer interface. The closed-form field expressions so obtained can then be directly used for the computation of the directivity function and the scattering matrix. The scattering matrix for the particular case of an electric dipole atop the confined chiral layer has been developed and used for the analysis of this structure's polarimetric response. The extension of this method to the analysis of multiple chiral layers and of anisotropic media is currently under way.

## References


[1] F. T. Ulaby and C. Elachi, *Radar Polarimetry for Geoscience Applications*. Norwood, MA, USA: Artech House, 1990.

[2] S. R. Cloude and E. Pottier, "An entropy based classification scheme for land applications of polarimetric SAR," *IEEE Trans. Geosci. Remote Sensing*, vol. 35, pp. 68-78, Jan. 1997.

[3] S. R. Cloude, J. Fortuny, J. M. Lopez-Sanchez, and A. J. Sieber, "Wide-band polarimetric radar inversion studies for vegetation layers," *IEEE Trans. Geosci. Remote Sensing*, vol. 37, pp. 2430-2441, Sept. 1999.

[4] S. R. Cloude, "Helicity in radar remote sensing," in *Proc. IGARSS 2002,* 2002, vol.1, pp. 411-413.

[5] S. J. S. Sant'Anna, J. C. S. Lacava, and D. Fernandes, "Closed form expressions for scattering matrix of simple targets in multilayer structures," in *Proc. IGARSS 2007,* 2007, pp. 714-717.

[6] S. J. S. Sant'Anna, J. C. S. Lacava, and D. Fernandes, "Evaluation of the scattering matrix of flat dipoles embedded in multilayer structures," *PIERS Online*, vol. 4, no. 5, pp. 536-540, 2008.

[7] S. J. S. Sant'Anna, "Electromagnetic scattering modeling of multilayer structures with applications in microwave remote sensing," Ph. D. thesis, Instituto Tecnológico de Aeronáutica (ITA), São José dos Campos, Brazil, May 2009. (In Portuguese).

[8] R. E. Collin and F. J. Zucker, *Antenna Theory*, Part 1. New York, McGraw-Hill, 1969.

[9] J. J. Van Zyl, H. A. Zebcker, and C. Elachi, "Imaging radar polarization signature: theory and observations," *Radio Science*, vol. 22, no. 4, pp. 529-543, 1987.